Cost-Effective Force Field Tailored for Solid-Phase Simulations of OLED Materials

M. Moral,[†] W.-J. Son,[‡] J. C. Sancho-García,[†] Y. Olivier,[¶] and L. Muccioli*[,§,‖]

[†]Departamento de Química Física, Universidad de Alicante, 03080 Alicante, Spain
[‡]Samsung Advanced Institute of Technology, Suwon, 443-803 Gyeonggi-do, South Korea
[¶]Laboratory for Chemistry of Novel Materials, University of Mons, 7000 Mons, Belgium
[§]Department of Industrial Chemistry "Toso Montanari", University of Bologna, 40136 Bologna, Italy
[‖]Laboratoire de Chimie des Polymères Organiques (LCPO), UMR 5629, University of Bordeaux, 33607 Pessac, France

Ⓢ Supporting Information

ABSTRACT: A united atom force field is empirically derived by minimizing the difference between experimental and simulated crystal cells and melting temperatures for eight compounds representative of organic electronic materials used in OLEDs and other devices: biphenyl, carbazole, fluorene, 9,9′-(1,3-phenylene)bis(9H-carbazole)-1,3-bis(N-carbazolyl)-benzene (mCP), 4,4′-bis(N-carbazolyl)-1,1′-biphenyl (pCBP), phenazine, phenylcarbazole, and triphenylamine. The force field is verified against dispersion-corrected DFT calculations and shown to also successfully reproduce the crystal structure for two larger compounds employed as hosts in phosphorescent and thermally activated delayed fluorescence OLEDs: N,N′-di(1-naphthyl)-N,N′-diphenyl-(1,1′-biphenyl)-4,4′-diamine (NPD), and 1,3,5-tri(1-phenyl-1H-benzo[d]imidazol-2-yl)phenyl (TPBI). The good performances of the force field coupled to the large computational savings granted by the united atom approximation make it an ideal choice for the simulation of the morphology of emissive layers for OLED materials in crystalline or glassy phases.
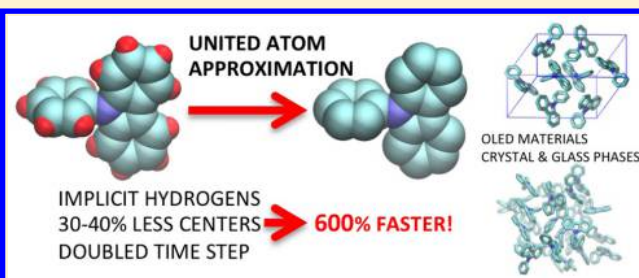
1. INTRODUCTION

Molecular and polymeric materials composed of recurrent aromatic moieties, such as phenyl and carbazolyl, are becoming ubiquitous in organic electronics applications[1] as donors and acceptors for organic solar cells,[2,3] metal-free dyes[4,5] or hole transporters[6] in Graetzel solar cells, host semiconducting,[7–12] and emitting materials in organic light-emitting diodes (OLEDs),[9,13–17] to name the most important ones. In particular, all the emissive, hole, and electron conducting (blocking) layers in small molecule and polymer OLEDs are often composed of nitrogen-rich units featuring an sp²- or sp³-hybridized nitrogen (e.g., carbazoles and amines).[7,18]

To rationally improve the efficiency of the emissive layer and to gain insight into the interplay between the host and guest electronic structures in particular, and to consequently access the rates governing hole–electron recombination and light emission processes, we used atomistic-like simulations combined with quantum chemistry calculations, which represent the most powerful theoretical method currently available.[19,20] However, high computational costs associated with such methodologies have to date prevented their application toward chemically detailed simulations of an OLED, which are typically modeled only at the macroscopic[21] or lattice level.[22,23]

Indeed, to investigate microscopically how structure affects the kinetic and energetic magnitudes determining efficiency in organic electronic devices, it is urgent to derive and employ force fields that not only reliably reproduce the physical properties of these materials but are also simple and efficient enough to grant the possibility of simulating the morphology of a whole emissive layer[19,20,24,25] (i.e., of samples with dimensions of approximately $10^4 - 10^6$ nm³). Note that the most popular force fields are optimized for other purposes[26] and that, to date, the literature appears to not only be scarce of efforts for obtaining the first objective, with an exception made for the notable work of Andrienko, Lennartz, Wenzel, and collaborators,[19,20,24,27–30] but also almost absent of attempts to reduce computational cost via the derivation of simpler potentials.

Below, we thus attempt to partially fill this gap by describing and tailoring a simple and computationally cost-effective united atom force field able to rather accurately reproduce the solid phase properties of some typical organic compounds employed in the OLED industry (Figure 1). This investigation is particularly timely because of the rise, besides transition metal-based phosphorescent emitters, of new all-organic ones with thermally activated[12,13,31–35] and aggregation-induced fluorescence[14–16,36] playing a major role, which are precursors to the realization of fully organic OLEDs, and thus it represents the ideal prosecution of our previous study on the accurate
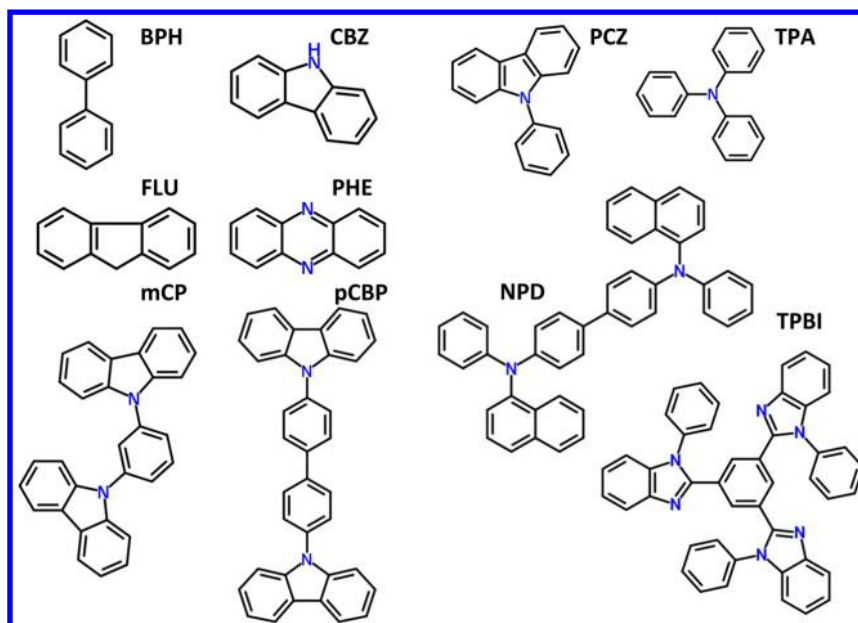
Figure 1. Chemical structures of the studied compounds, including biphenyl (BPH), carbazole (CBZ), fluorene (FLU), 9,9′-(1,3-phenylene)bis(9H-carbazole)-1,3-bis(N-carbazolyl)benzene (mCP), 4,4′-bis(N-carbazolyl)-1,1′-biphenyl (pCBP), phenazine (PHE), 9-phenyl-9H-carbazole (PCZ), and triphenylamine (TPA), forming the training set used for the empirical parametrization, whereas N,N′-di(1-naphthyl)-N,N′-diphenyl-(1,1′-biphenyl)-4,4′-diamine (NPD) and 1,3,5-tri(1-phenyl-1H-benzo[d]imidazol-2-yl)phenyl (TPBI) were simulated only to test the optimized version of the force field. The H atoms and the corresponding C−H bonds are omitted for clarity.

theoretical calculation of singlet−triplet energy gaps for this class of materials.[34]

2. MOLECULES AND INITIAL SETUP OF THE FORCE FIELD

We started by selecting eight small molecules of known crystal cell structure, as shown in Figure 1: BPH, CBZ, FLU, mCP, pCBP, PHE, PCZ, and TPA.[37] All of these molecules are either used as host OLED materials themselves (e.g., PCZ, TPA, and CBZ) or constitute recurring chemical units in more complex polymeric or molecular structures.[18,38] We then proceeded to the setup of a united atom (UA) force field able to adequately reproduce the crystal structure of the selected compounds. The choice of UA representation, also known as "extended atom" approximation, is justified by the large savings of computational time it allows at the cost of a minimal loss of accuracy and of some extra effort in its parametrization.[39] In a nutshell, every aliphatic or aromatic hydrogen atom is modeled only implicitly,[40] and its mass is summed to that of the carbon atom to which it is bonded. Such a customization of the force field can indeed turn into a long exercise requiring several steps.[41] Here, we started by adopting the widely used AMBER-like or CHARMM-like potential energy function[42]

$$U_{\text{total}} = \sum_{\text{bonds}} K_r^*(r - r_e^*)^2 + \sum_{\text{angles}} K_\theta^*(\theta - \theta_e^*)^2$$
$$+ \sum_{\text{dihed}} \sum_{n^*} V_n^*[1 + \cos(n^*\phi + \gamma_n^*)] + \sum_{\text{improper}} K_\phi^*(\phi - \phi_e^*)^2$$
$$+ \sum_{\text{atoms}} \left\{ 4\sqrt{\epsilon_i^* \epsilon_j^*} \left[\left(\frac{\sigma_i^* + \sigma_j^*}{2r_{ij}} \right)^{12} - \left(\frac{\sigma_i^* + \sigma_j^*}{2r_{ij}} \right)^6 \right] + \frac{q_i^* q_j^*}{r_{ij}} \right\}$$

(1)

where, for clarity, all of the parameters have been starred. For the harmonic constants K_r and K_θ, we rely on the AMBER95 parameter set,[43] whereas the corresponding equilibrium

distances and angles r_e and θ_e, respectively, were adjusted comparing their equilibrium molecular mechanics geometries with the ones produced by highly accurate calculations. The torsional parameters V_n, n, γ_n were borrowed from the AMBER95 data set for those concerning the rigid ones (e.g., torsions involving carbon atoms belonging to the same aromatic ring), whereas soft, anharmonic torsions were parametrized here with quantum chemistry calculations[29,41,44] at the PBE0-D3(BJ)/def2-TZVP level. In practice, only three types of torsion were reworked: phenyl−phenyl, phenyl−carbazole, and the improper torsion involving the out-of-plane vibration of sp² nitrogen; the phenyl−nitrogen torsion in TPA was modeled with standard parameters because it is dominated by steric repulsion, which confers to this molecule propeller-like structure.[45] Fully relaxed scans of the potential energy surface as a function of the dihedral angle were run in steps of 5 degrees, using BPH and PCZ as target fragments, with the obtained profiles shown in Figure 2. It is worth noting that these torsions are also present in the largest compounds of the training set, namely mCP and pCBP, and in many other OLED materials.[18,38]

The force field parameters matching the torsional potentials were optimized with the procedure described in ref 44, consisting of deriving the free energy torsional profile with adaptive biasing force MD runs[46] and fitting the difference between QM and MD with a cosine series (see eq 1). Turning to the Lennard-Jones (LJ) parameters σ and ϵ entering the last term of eq 1, nine atom types were first identified (i.e., chemically equivalent atoms sharing the same parameters, see Tables 1 and 2), and their initial values were set to the ones found in literature (refs 43 and 47−49). As is customarily done,[42,50] the atomic charges q were derived by fitting the molecular electrostatic potential obtained by quantum chemistry calculations. For this purpose, the PBE0-D3(BJ)/def2-TZVP model chemistry was adopted[51−55] with numerical thresholds systematically increased with respect to defaults and dispersion corrections -D3(BJ),[56] because as we have reported recently, it shows good all-around performances
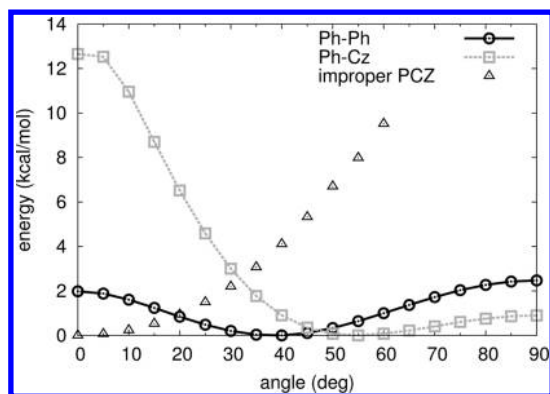
Figure 2. Quantum mechanical potential for the phenyl−phenyl dihedral angle in BPH (circles), phenyl−carbazole dihedral angle in PCZ (squares), and improper dihedral carbazole-*N*-phenyl in PCZ (triangles) systematically calculated at the PBE0-D3(BJ)/def2-TZVP level[34] by fully relaxing the geometry while keeping the dihedral angle fixed.

for some of the compounds studied here as well as for some emitters exhibiting thermally activated delayed fluorescence (see ref 34 for further details). Molecular geometries were first optimized by PBE0/def2-TZVP calculations, and then the charges on the heavy atoms were calculated at the PBE0/TZVP level with the electrostatic potential fitting algorithm[57] implemented in the Gaussian 09 package.[58] All the other quantum mechanics calculations were performed with the ORCA code, version 3.0.0.[59] All of the atomistic simulations were run with the NAMD 3.0 software.[60] The trajectories were analyzed with in-house written Fortran 95 code.

3. COMPUTATIONAL STRATEGY

For each target compound, a supercell was created by replicating the experimental crystal cell along its *a*, *b*, and *c* axes to thus have at least three replica per side and supercell sides as close as possible to 5 nm to realize a sensible compromise between finite size effects and computational costs. With these criteria, the sample sizes range from approximately 6000 to 10000 atoms, corresponding to $N = 540$ (BPH, $6 \times 9 \times 5$ supercell),[62] 756 (CBZ, $7 \times 3 \times 9$),[63] 756 (FLU, $7 \times 3 \times 9$),[64] 288 (mCP, $6 \times 4 \times 3$),[65] 180 (pCBP, $6 \times 3 \times 5$),[66] 560 (PHE, $7 \times 10 \times 4$),[67] 360 (PCZ, $3 \times 5 \times 3$),[68] and 432 (TPA, $3 \times 3 \times 3$)[69] molecules per simulation box, respectively. For each parameter set, supercells were equilibrated with molecular dynamics at a constant volume for 0.4 ns and then at atmospheric pressure for 2 ns, and finally, the density and box sizes were averaged over a further 1 ns-long run; the simple velocity scaling thermostat and Berendsen's barostat were used in all of the runs. Simulated temperatures for

Table 2. Starting Values of Lennard-Jones Parameters σ and ϵ for Each Atom Type and Corresponding Reference ("Start" Force Field) and Percent Variation of the Radii σ for the Heuristic R1, R2, and R3 Force Fields

name	σ (Å)	ϵ (kcal/mol)	ref	R1	R2	R3
C2	3.70	0.1094	48	+10%	+10%	+10%
CA	3.43	0.0860	50	+2%	+4%	+4%
CH	3.56	0.1114	49	+3%	+4%	+4%
CX	3.43	0.0860	50		−4%	−4%
CY, CW	3.43	0.0860	50	+4%	+4%	+5%
N	3.28	0.1700	50	+5%	+4%	
NH	3.28	0.1700	50	+5%	+4%	+4%
N3	3.28	0.1700	50	+5%	+4%	+4%
N4, N5[61]	3.28	0.1700	50	+5%	+4%	

each compound correspond to those of the measurements of experimental crystal structures as downloaded from the Cambridge Structural Database (CSD; entries BIPHEN04, CRBZOL04, FLUREN01, NEPWUB, KANYUU, PHENAZ04, PEMWEJ, and ZZZJCQ01) typically at room temperature (set to 293 K for BPH, FLU, PHE, PCZ, and TPA) or below (168 K for CBZ, 291 K for mCP, and 120 K for pCBP), and the pressure is always fixed to 1 atm.

To be able to quantitatively compare the results of two different force fields, and eventually to systematically vary the FF parameters to match the experimental results, it is necessary to define an appropriate scoring function. Here, the deviation of the simulated cell from the experimental one was measured as

$$F = \frac{1}{2}(\Delta_{\text{vol}} + \Delta_{\text{def}}) \tag{2}$$

which accounts, through the function Δ_{vol}, for the variation of the volume of the simulated cell (subscript s) with respect to the experimental cell (subscript e), and for the deformation of the cell shape through Δ_{def}

$$\Delta_{\text{vol}} = \frac{1}{3} \frac{|V_e - V_s|}{V_e} \tag{3}$$

$$\Delta_{\text{def}} = \frac{1}{3}\left[\prod |\cos(\delta_e^i - \delta_s^i)|^{-1} \prod \left(1 + \frac{|l_e^i - l_s^i|}{l_e^i}\right) - 1 \right] \tag{4}$$

where $l^i = a, b, c$ and $\delta^i = \alpha, \beta, \gamma$ are the crystal cell axes and angles, respectively, and $V = abc\,(1 - \cos^2 \alpha - \cos^2 \beta - \cos^2 \gamma + 2 \cos \alpha \cos \beta \cos \gamma)^{1/2}$ is the volume of the crystal unit cell. So as not to bias the scoring functions toward systems with smaller unit cells, for which the absolute variations of volume and cell sides are obviously smaller, both Δ_{vol} and Δ_{def} are dimensionless

Table 1. Atom Types Included in the Force Field and Their Occurrence for Each Molecule of the Training Set

name	description	BPH	CBZ	FLU	mCP	pCBP	PHE	PCZ	TPA
C2	-CH$_2$- group			1					
CA	aromatic C		2	2	4	4	4	4	
CH	ua aromatic C−H group	10	8	8	16	28	8	11	15
CX	bridge aromatic C	2	2	2	4	6			
CY	aromatic C bonded to sp^2 N				2	2		1	3
N	aromatic sp^2 N						2		
NH	carbazole NH group		1						
N3	sp^2 N (e.g., in PCZ)				2	2		1	
N4	triphenylamine sp^3 N								1

quantities. In practice, F is zero for a perfect agreement between experimental and simulated values and is otherwise greater than zero. For the simple case of an isotropic deformation of the experimental cell (i.e., $l_s^i = \lambda l_e^i$), F takes the value of $|\lambda - 1|$ for $\lambda \to 0$; hence, small values of F can be assimilated into the strain of the simulated cell with respect to the experimental cell.[70]

4. OPTIMIZATION OF LENNARD-JONES RADII

In a classical force field, the intermolecular forces responsible for the cohesive energy in the crystal phase are represented by a Lennard-Jones and an electrostatic term (see last summation in eq 1). Considering that atomic point charges are directly derived from DFT calculations, which are accurate enough in the description of the molecular charge density,[71] our empirical exploration was limited to optimizing the Lennard-Jones parameters (ϵ and σ, see Tables 1 and 2), which conversely are very difficult to evaluate accurately by purely theoretical means.[72,73]

With the initial parameter set taken from the literature and customized with QM charges and dihedrals, an average score of 0.027 is obtained, which is a rather unsatisfactory value as it translates to overestimations of the densities as large as 0.12 g/cm³ with the exception of BPH. The observation of BPH being an outlier, which is confirmed for almost all of the attempted parametrizations, is not surprising as it is known that the intermolecular interactions for benzene and short oligophenyls are particulary difficult to model with classical, nonpolarizable force fields,[74] and special parameters are often required to obtain good accuracy.[75,76] In addition, the united atom approximation, which eliminates the aliphatic hydrogens and their point charges, yields a poor description of the electric quadrupoles of the phenyl rings.[77]

Furthermore, the global overestimation of the densities with standard parameters can be easily rationalized, recalling that the OPLS LJ parameters are optimized for the simulation of liquids[78] and not for the solid state. This statement can be supported with an example, whereby it is worth noticing that the LJ parameters reported in Table 2 give satisfactory results in modeling the liquid crystal phases of metal-free phthalocyanines,[79] whereas conversely they yield a rather poor description of poly-3-hexyl-thiophene crystalline domains.[80] Interestingly, a similar over-estimation of the experimental density was observed for the latter system: in that case, the bias was corrected by increasing the σ of the aliphatic carbons of the hexyl chains by 8%.[80] Here, we applied the same strategy. After having assessed that small variations of the various ϵ do not significantly alter the scoring function, as shown in Figure S1 in the Supporting Information, we proceeded with a systematic increase in the atom sizes σ for the atom types as shown in Table 1, starting from the most abundant ones (CA and CH).

Upon inspecting Figure 3, it can be appreciated how the strategy of progressively modifying the σ parameters is successful: although no improvement is obtained by decreasing σ for CA or CH; conversely, an increase of 2−4% significantly reduces the average score from the initial value of 0.027 to a more acceptable 0.018. It is also useful to observe in Figure 3 (see also Figures S1 and S2 in the Supporting Information) that the most important contribution to the total score comes from the anisotropic deformation term Δ_{def}, which cannot be decreased as Δ_{vol} by uniformly scaling all of the atom sizes. Therefore, once this stage of optimization was reached, we started from the "CH + 4%" force field and applied some heuristic changes to the radii of other atom types by considering their relative occurrence
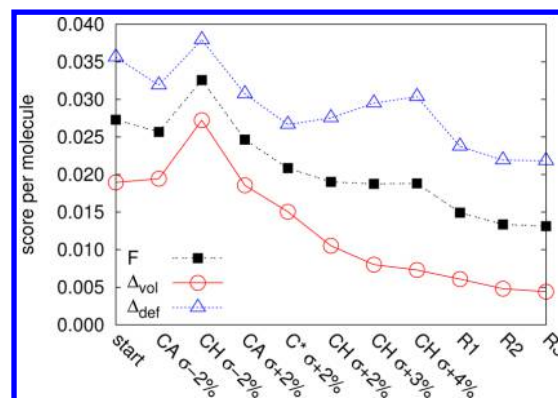
Figure 3. Performance of the different parametrizations obtained by varying the LJ radii. C* stands for all carbon atom types. R1, R2, and R3 are further refinements of the "CH σ + 4%" force field, as described in the text.

(Table 1) and the separate scores of the different molecules in the training set (see Figure S2 in the Supporting Information), obtaining three refined parametrizations, labeled R1, R2, and R3, as detailed in Table 2. These attempts further reduced the score, namely to a minimum of ∼0.013 for the R3 case, which was selected accordingly as the force field for further optimization. As shown in Table 3, with this parametrization, all of the simulated cell parameters and densities, except BPH, are very close to their experimental counterparts (RMSD 0.32, 0.16, and 0.43 Å for a, b, and c, respectively, and 0.026 g/cm³ for density).

5. TUNING OF LENNARD-JONES POTENTIAL WELL DEPTHS

Following the observation in the previous section that the structure of the crystal cell is only weakly infuenced by changes in the potential well depth ϵ, we next tackled the optimization of the σ parameters for accurately reproducing the experimental crystal structures. However, at this stage, the ϵ values were left unoptimized, still demanding an alternative physical property. For this purpose, we chose the melting points of the target compounds because they are a good indicator of intermolecular cohesion energy in the crystal, and attempted some scaling of the ϵ to maximize the agreement with the experimental data. A possible alternative would have been to choose boiling points, but this property might not be available for the large compounds typically used in OLEDs, and in addition, they are less relevant for OLED processing because they are often too high and far from room temperature. Melting points are determined in a straightforward manner with computer simulations by heating the crystal at increasing temperature until achieving the isotropic liquid phase, though hysteresis and system size may play an important role, typically leading to an overestimation of the actual melting temperature.[81,82] Here, we used the supercells described in the previous sections as starting configurations and equilibrated them for 3 ns at each simulated temperature at atmospheric pressure. The temperature scan was performed at intervals of 25 K, typically starting at 300 K. As an operational definition of the melting point, the lowest temperature at which the sample becomes orientationally isotropic after 3 ns of simulation was considered. An example of the typical character-ization of the phase change in terms of density, orientational order parameter, translational diffusion coefficient, and radial distribution is reported in the Supporting Information.

Table 3. Experimental (e) and Simulated (s) Unit Cells with the United Atom R3 and R3 $\epsilon - 8\%$ Force Fields and Full Atom (FA)[a] and T-FA[b] Force Fields[c]

| compound	FF	ρ	V	a	b	c	α	β	γ	F ($\times 10^2$)
BPH	e	1.18	435.8	8.12	5.63	9.51	90.0	95.1	90.0	0.0
	s R3	1.12	460.5	8.64	5.67	9.38	90.0	95.5	90.0	2.4
	s R3 $\epsilon - 8\%$	1.10	470.0	8.89	5.60	9.42	90.0	95.6	90.0	3.2
	s FA	1.14	451.1	8.62	5.40	9.67	90.0	95.3	90.0	2.6
	s T-FA	1.15	449.9	8.54	5.43	9.68	90.0	95.3	90.0	2.3
CBZ	e	1.36	818.5	7.63	18.93	5.66	90.0	90.0	90.0	0.0
	s R3	1.34	827.0	7.63	18.73	5.78	90.0	90.0	90.0	0.7
	s R3 $\epsilon - 8\%$	1.34	827.8	7.62	18.74	5.79	90.0	90.0	90.0	0.8
FLU	e	1.20	917.6	8.47	18.92	5.72	90.0	90.0	90.0	0.0
	s R3	1.21	917.3	8.31	18.72	5.89	90.0	90.0	90.0	1.0
	s R3 $\epsilon - 8\%$	1.20	923.6	8.34	18.75	5.90	90.0	90.0	90.0	1.1
mCP	e	1.26	2159.7	9.07	12.50	19.04	90.0	90.0	90.0	0.0
	s R3	1.26	2161.7	9.59	12.40	18.17	90.0	90.0	90.0	1.9
	s R3 $\epsilon - 8\%$	1.25	2168.2	9.60	12.39	18.22	90.0	90.0	90.0	2.0
pCBP	e	1.31	1314.1	8.01	16.01	10.24	90.0	110.2	90.0	0.0
	s R3	1.34	1293.3	8.16	16.03	9.88	90.0	111.4	90.0	1.2
	s R3 $\epsilon - 8\%$	1.34	1295.9	8.16	16.03	9.90	90.0	111.3	90.0	1.1
	s FA	1.20	1420.2	8.42	14.97	11.26	90.0	109.3	90.0	5.2
	s T-FA	1.29	1373.9	9.47	14.63	9.91	90.0	114.9	90.0	6.3
PHE	e	1.33	460.1	7.08	5.07	12.79	90.0	102.3	90.0	0.0
	s R3	1.32	463.8	6.73	5.09	13.51	90.0	101.1	90.0	0.2
	s R3 $\epsilon - 8\%$	1.31	466.2	6.74	5.12	13.48	90.0	101.1	90.0	2.1
PCZ	e	1.22	2887.0	14.53	10.98	18.09	90.0	113.5	90.0	0.0
	s R3	1.24	2861.8	14.88	10.64	18.07	90.0	114.1	90.0	1.1
	s R3 $\epsilon - 8\%$	1.23	2876.9	14.90	10.67	18.09	90.0	114.1	90.0	1.0
	s FA	1.15	3126.9	16.24	10.53	18.28	90.0	116.1	90.0	4.3
	s T-FA	1.22	2868.6	14.48	10.54	18.79	90.0	112.5	90.0	1.5
TPA	e	1.18	5512.2	15.66	22.26	15.81	90.0	90.0	91.0	0.0
	s R3	1.19	5485.4	15.64	22.18	15.81	90.0	90.0	91.0	0.1
	s R3 $\epsilon - 8\%$	1.18	5538.9	15.73	22.17	15.88	90.0	90.0	91.0	0.3
NPD	e	1.23	1691.9	10.30	11.33	14.49	82.4	77.7	75.6	0.0
	s R3 $\epsilon - 8\%$	1.26	1649.4	10.18	11.42	14.18	82.3	77.5	75.8	1.1
TPBI: CH_3-OH	e	1.25	3735.2	11.25	18.69	17.76	90.0	101.6	90.0	0.0
	s R3 $\epsilon - 8\%$	1.25	3722.2	11.01	18.23	18.54	90.0	100.9	90.0	1.6

[a]AMBER95 plus PBE0/def2-TZVP point charges. [b]Identical to FA but with reparameterized dihedrals. [c]Densities (ρ) are expressed in g/cm^3, cell volumes in Å^3, sides in Å, and angles in deg. The angles that are equal to 90 deg in the experimental cell are kept fixed to this value during the simulation. The overall quality of the result is evaluated with the F score (eqs 2−4).

Table 4. Melting Points (K) for the Studied Compounds As Obtained by Systematically Rescaling the Original LJ Energy Well Depths ϵ of All Atom Types and Using the Radii of the R3 Parameter Set, along with the Corresponding Crystal Structure Score F and Mean Absolute Deviation between Experimental and Simulated Melting Temperatures ($|\Delta T| = \sum_{i=1}^{8} |T_e^{m,i} - T_s^{m,i}|/8$, in K)

compound	EXP[86]	R3	+10%	−5%	−8%	−10%	−15%	−20%
BPH	342	325	350	325	300	300	300	275
CBZ	518	700	750	675	675	650	625	600
FLU	386	550	600	525	525	500	500	475
mCP	449	725	775	700	700	700	650	650
pCBP	556	950	1050	900	875	850	825	775
PHE	447	650	675	625	600	600	575	550
PCZ	369	550	600	525	525	525	475	425
TPA	399	475	525	475	475	450	425	400
$|\Delta T|$	0	187	232	165	162	149	124	102
F ($\times 10^2$)	0	1.31	1.32	1.34	1.44	1.90	1.92	2.05

Clearly, this is just a coarse measurement that is expected to produce an overestimation of melting points because the interval of 25 K is rather large and the sampling time of 3 ns may be too short for the process to occur at temperatures close to the melting point. Once melting points were estimated, the performance of each force field was evaluated by means of the absolute deviation between experimental and simulated values ($|\Delta T| = \sum_{i=1}^{8} |T_e^{m,i} - T_s^{m,i}|/8$); on the basis of the previous considerations of the melting point determination, any value below 50 K can be considered a very good score. In attempting
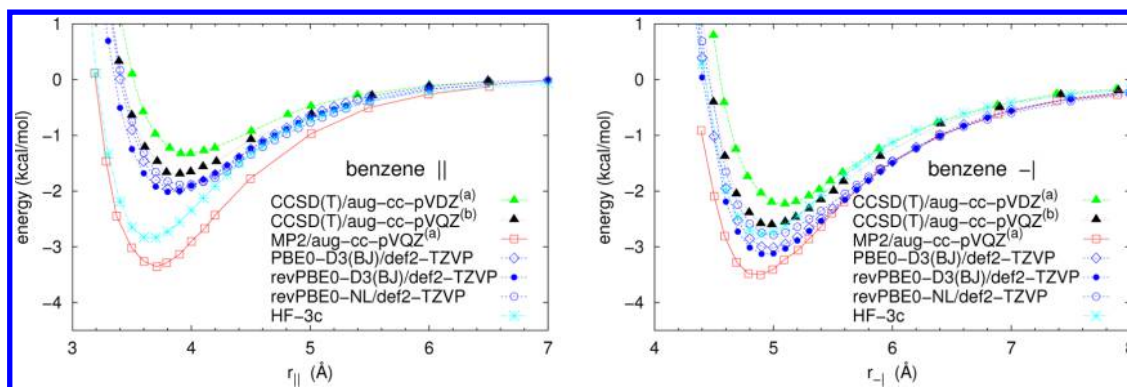
Figure 4. Calculated intermolecular energies for two cofacial (left) and "T" oriented (right) benzene molecules. MP2 and CCSD(T) data are extracted from ref 89. (a) Counterpoise corrected values. (b) Values estimated from counterpoise-corrected CCSD(T)/aug-cc-pVDZ and MP2/aug-cc-pVDZ calculations.

this evaluation, it is also important to take into account that there is no guarantee that a classical force field able to simultaneously reproduce the experimental melting point and crystal structure exists. For instance, it is possible that altering ϵ may also increase the crystal cell scoring function F.

From Table 4, which reports the scores for all attempts at scaling the ϵ parameters, we observe that, luckily, this is not the case for changes up to 10% with respect to the initial values, but that conversely, the melting points are largely overestimated by the force fields. The scores also show that all variations of the R3 force field proposed here overestimate the boiling points of the target molecules with the usual exception of BPH. To decrease the boiling points, the interaction between atoms must be decreased, and hence ϵ must be reduced, but with the constraint that the reproduction of the experimental crystal structure must not become worse, as monitored through the F scoring function. In our case, we found that the best compromise is obtained by scaling to 92% of the original interaction strengths (Table 2). We label this force field "R3 $\epsilon - 8\%$". By the results presented in Table 3 again, we notice that the performances are slightly lower than those of R3, whereas the melting temperatures obtained for the scaled force field are at least 20 K closer to the experimental values. Using this parametrization, we also computed the surface energies for crystal planes (100), (010), and (001) and for glassy samples obtained by freezing and equilibrating the liquid samples obtained above (see Figure S5 and Table S5 in the Supporting Information for further details). Such energies vary in a range between 0.05 and 0.15 J/m^2 for the crystal phase, in line with calculated[83,84] and experimental data[85] for other organic crystals. Conversely, they are almost halved in the glass phase (0.05−0.08 J/m^2), reflecting the lower internal energy of the bulk glass phase with respect to the bulk crystal.

6. ADDITIONAL TESTS FOR THE INTERMOLECULAR POTENTIAL

As a further quality check of the R3 $\epsilon - 8\%$ force field, we compared its prediction for selected intermolecular potential energy curves with the ones produced by state-of-the-art dispersion-corrected density functional theory (DFT) methods[73] with the latter specifically including the correct dependence on the internuclear separation at large distances (i.e., the so-called long-range behavior). For this purpose, we selected the well-rounded Perdew−Burke−Ernzerhof (PBE) functional in its standard hybrid (PBE0) and revised (revPBE0) versions[51−54] with the rather large (nearly converged) def2-TZVP basis set;

regarding the dispersion corrections, we employed either the -D3(BJ) function[56] or the -NL (van der Waals) approach[87] to separately disentangle the effect (if any) of both the functional form and the dispersion correction used. In addition, we tested the recently developed HF-3c method (computationally inexpensive compared to other DFT-based methods), which includes Kruse and Grimme's geometric counterpoise corrections (gCP), the -D3(BJ) dispersion correction again, and a short-range basis incompleteness (SRB) correction for systematically overestimated bond lengths of electronegative elements when employing small basis sets.[88] The level of accuracy of the above theoretical methods was first verified by comparison with high level calculations published by Sherrill and co-workers using accurate (nearly converged) methods, such as CCSD(T)/aug-cc-pVDZ, CCSD(T)/aug-cc-pVQZ, and MP2/aug-cc pVQZ, all of which include counterpoise correction (CP) to reduce the well-known basis set incompleteness error typical of these calculations as much as possible.[89] In particular, the classical cofacial and "T" geometries were explored for a pair of benzene molecules, and the corresponding intermolecular energies were calculated as a function of the distance between the centers of mass of the two interacting molecules (Figure 4). PBE0 and revPBE0 give very similar energies, whereas the choice of the dispersion correction, -D3(BJ) or -NL, seems more critical, with -NL providing systematically weaker interaction energies with respect to -D3(BJ), and thus getting closer to the CCSD(T) reference values. HF-3c is in line with the more accurate methods for the T configuration, but instead largely overestimates the maximum interaction energy and underestimates the distance at which the cofacial interaction is maximum. This occurs also for PBE0 and revPBE0 calculations for both benzene−benzene configurations to a much lower extent, though not negligible in terms of percentage, particularly for the energies (for all the values of "equilibrium" distances and energies, see Tables S1−S4 in the Supporting Information). It can then be preliminarily concluded that, for small aromatic molecules, dispersion-corrected PBE0/def2-TZVP calculations (independent of the correction used) give semiquantively accurate results for energies, and quantitatively for distances, whereas the computationally cheaper HF-3c cannot be considered reliable enough, at least for π-stacking energies, such as in the case of the benzene cofacial dimer.

We then proceeded to the evaluation of intermolecular energies for molecular pairs of BPH and TPA (see Supporting Information for PCZ), in this case comparing quantum chemistry calculations with molecular mechanics. These
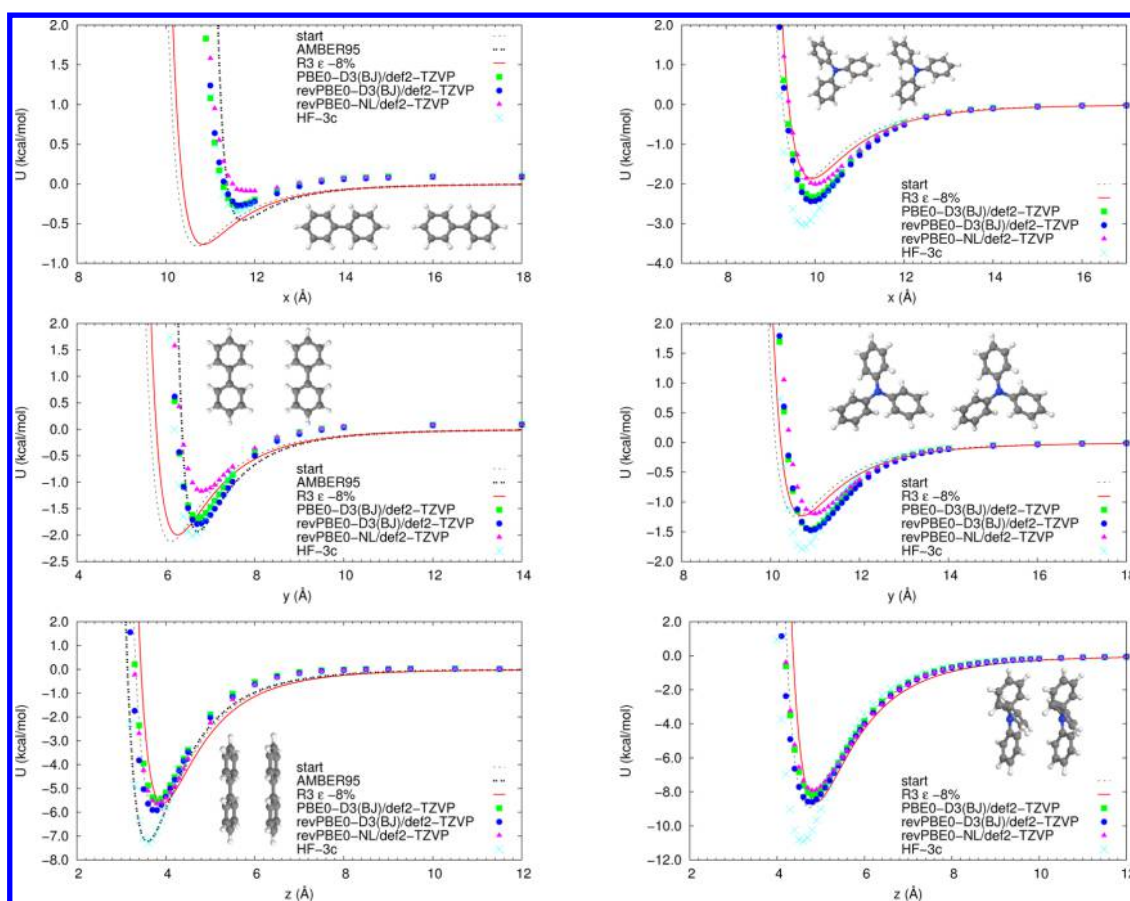
Figure 5. Calculated intermolecular energies for two parallel biphenyl molecules displaced along their *x*, *y*, and *z* inertia axes (left) and corresponding energies for two triphenylamine molecules (right).

molecules, at their experimental geometries in the crystal phase, were rotated into their principal inertial frame and superimposed. One of them was kept fixed, while the second was moved along the three Cartesian directions corresponding to the orientation of the inertia axes with increasing eigenvalue. Starting with the extreme case of biphenyl (Figure 5, left), we notice that all the quantum chemistry methods give approximately the same prediction for the minimum energy distance, whereas both the "start" and "R3 $\epsilon - 8\%$" provide a rather large underestimation (~1 Å) for the *x* and *y* displacement directions. The rationale of this behavior can be found in the united atom approximation. As shown by the snapshots on the left side of Figure 5, the *x* and *y* directions correspond to hydrogen−hydrogen contacts. These hydrogens are not present in the united atom force fields, where they are only partially compensated for by a larger van der Waals radius on the corresponding carbon; hence, these force fields underestimate the distance and overestimate the interaction. As further proof, we computed the same potential energy with the standard AMBER95/OPLS full atom parameters (black two-dashed lines), which conversely adheres to the ab initio curves. On the contrary, the *z* (π-stacking) direction is not affected by the united atom approximation, and here, both the "start" and "R3 $\epsilon - 8\%$" perfectly agree with the DFT values, whereas, as expected, HF-3c, and more surprisingly AMBER95, overestimate the attraction between the two parallel BPH molecules. Moving to the larger and more isotropic TPA molecule, the curves on the right side of Figure 5 show that, in this case, united atom approximation is harmless and that the united atom FFs agree with the dispersion-corrected DFT values, whereas HF-3c

performs poorly, constantly overestimating the interaction energies. As an additional comment, it is worth noting that (i) the small differences between the "start" and "R3 $\epsilon - 8\%$" FF results are always comparable or lower than the differences between one dispersion-corrected DFT calculations and another, and (ii) the very similar performance of the two FFs for the computation of interaction potential curves contrasts with their different capabilities of reproducing the crystal cells of the target compounds. It rather appears from these results that, for the time being, DFT-derived potential energy curves cannot be used as a reference method for parametrizing force fields[90] and that empirical tuning remains a more viable method.

For achieving further validation of the "R3 $\epsilon - 8\%$" FF parameters, we repeated the simulation scheme described in section 3 for two molecules outside the training set for which the experimental crystal structure is known: *N,N'*-bis(1-naphthyl)-*N,N'*-diphenyl-1,1'-biphenyl-4,4'-diamine (NPD; 5 × 4 × 3 supercell,[91] *N* = 120 molecules, 5520 centers, CSD entry: REHJAQ01) and 2,2',2″-benzene-1,3,5-triyltris(1-phenyl-1*H*-benzimidazole) (TPBI; cocrystal with methanol, 4 × 3 × 3 supercell,[92] *N* = 284 molecules for each species, 7776 centers, CSD entry: QUCJAA). Again, wherever necessary, soft torsional potentials where reparametrized (see Figure S4 in the Supporting Information), and united atom charges were calculated for each center for both molecules (see Supporting Information). In Table 3, it can be seen that, for these two example molecules, the quality of the reproduction of the experimental cells is good and comparable to the one achieved for the molecule belonging to the training set, suggesting that the

Lennard-Jones parameters derived in this work could be safely transferred to other similar compounds.

To conclude, it is also worth assessing whether the parametrization exercise is just a consequence of opting for the united atom approximation, and also if this approximation is actually useful for saving precious computational time. For doing this, we chose the most complex molecule in the training set, pCBP, and set up a full atom force field by this time employing the full atom PBE0/def2-TZVP charges and the popular GAFF parameters for Lennard-Jones and intramolecular parameters.[50] We produced two versions of this force field: one without reoptimizing the dihedral parameters (labeled FA in Table 3), and a second one (T-FA) where the phenyl−phenyl, phenyl−carbazole, and improper sp^2 nitrogen dihedrals were refined with ab initio data, exactly as described above for the united atom FF. As this reoptimization requires the simulation of BPH and CBZ as well, we also reported in Table 3 the results corresponding to their crystal cells. Starting with the difficult case of BPH, it appears that the full atom picture does not particularly improve the simulation result, independently of the dihedral potential: the density gets closer to the experimental value, but the value of the b side decreases with respect to the experimental value (and to the united atom FFs). For CBZ instead, the reparametrization of the dihedral seems very relevant: the full atom F score drops from a very poor 0.043 to 0.015 because of it; however, the optimized united atom FFs perform slightly better. For pCBP, the comparison is even more rewarding for the united atom force fields, which give scores of ∼0.01 versus 0.05−0.06 for the full atom ones, thus confirming the necessity of tailoring the LJ parameters for solid state simulations. Finally, these tests provided us with an estimate of the computational savings brought by the united atom approximation, consisting of an appreciable factor of ∼6× (0.4 days/ns vs 2.5 days/ns for pCBP on a single logical core of an Intel Xeon E5-2620v2 2.1 GHz processor).

7. CONCLUSIONS

In summary, we derived a simple molecular mechanics force field aimed at the accurate and computationally efficient simulation of the morphology of materials used in the realization of organic light-emitting diodes. To increase awareness for potential users, we recap here the main approximations, limitations, and good practices for safe application of the force field parameters:

● The force field relies on the united atom approximation, where hydrogens are only implicitly accounted for, which grants an acceleration of ∼600%, but also results in a lack of accuracy for describing specific contacts (see Figure 5) and cannot be used for hydrogen-bond forming systems.

● DFT calculations at the PBE0-D3(BJ)/def2-TZVP level were performed for the parametrization of the point charges on each united atom center and for the soft torsional potentials between rigid aromatic units; similar calculations are required for any new compound to be studied.

● The Lennard-Jones parameters were empirically optimized to maximize the agreement with available experimental data, namely, crystal cell shape and size, as well as the melting temperatures for a training set of eight compounds.

● As the main empirical tuning of the parameters was performed to match the experimental crystal (hence, a solid phase), we hypothesize that the parametrization will also be effective in reproducing another solid phase: the glassy one typically found in OLED devices.

● It is probably impossible to obtain a classical and simple force field "for all seasons",[93] for instance, coarse-grained force fields for polymers only work close to the temperature and pressure from which they are derived,[94] and different force fields are required to reproduce high and low pressure benzene polymorphs.[95] In our specific case, reproduction of the boiling point is not satisfactory; consequently, we discourage the application of the force field for simulations of bulk liquid phases.

● The transferability of the force field was demonstrated by performing the simulation in crystal phase of two compounds outside the training set, whose results were again in good agreement with experimental data. This result, although promising, is not sufficient to ensure the transferability to other compounds, in particular, if they contain new chemical moieties. In that case, the best practice would be to benchmark the force field against the experimental crystal structure, if available, or versus any other experimental data.

Having listed all of the limitations of the proposed methodology, it is also worth stressing that the good reproduction of physical properties in the solid state, together with the large computational savings expected with respect to full atom force fields, make the force field presented here a suitable candidate for simulating the morphology of emissive layers for OLED materials consisting of thousands of molecules, paving the way toward their computational screening in a multiscale approach.

■ ASSOCIATED CONTENT

Ⓢ Supporting Information

(S1) Effect of scaling the Lennard-Jones ϵ parameters on the scoring function, (S2) compound-wise performances of the different parametrizations, (S3) intermolecular potential energy curves for PCB, (S4) torsional energy profiles for NPD- and TPBI-specific dihedral angles, (S5) glass transition temperature determination for the target compounds, (S6) example of the characterization of the crystal−liquid phase transition; tables with fit parameters of benzene, BPH, PCZ, and TPA intermolecular energies with Morse equation, and calculated surface energies for crystalline and glassy samples; archive containing CHARMM topology and parameter files (united atom R3 ϵ − 8% and full atom T-FA), typical NAMD configuration file, and PDB files for united atom and full atom crystal cells. The Supporting Information is available free of charge on the ACS Publications website at DOI: 10.1021/acs.jctc.5b00164.

■ AUTHOR INFORMATION

Corresponding Author
*E-mail: Luca.Muccioli@u-bordeaux.fr.

Notes
The authors declare no competing financial interest.

■ ACKNOWLEDGMENTS

■ REFERENCES

(1) Boudreault, P.-L. T.; Beaupre, S.; Leclerc, M. *Polym. Chem.* **2010**, *1*, 127−136.

(2) Gendron, D.; Leclerc, M. *Energy Environ. Sci.* **2011**, *4*, 1225−1237.

(3) Barito, A.; Sykes, M. E.; Huang, B.; Bilby, D.; Frieberg, B.; Kim, J.; Green, P. F.; Shtein, M. *Adv. Energy Mater.* **2014**, *4*, 1400216.

(4) Mishra, A.; Fischer, M. K. R.; Bäuerle, P. *Angew. Chem., Int. Ed.* **2009**, *48*, 2474−2499.

(5) Yeh-Yung Lin, R.; Lin, H.-W.; Yen, Y.-S.; Chang, C.-H.; Chou, H.-H.; Chen, P.-W.; Hsu, C.-Y.; Chen, Y.-C.; Lin, J. T.; Ho, K.-C. *Energy Environ. Sci.* **2013**, *6*, 2477−2486.

(6) Zhou, N.; Lee, B.; Timalsina, A.; Guo, P.; Yu, X.; Marks, T. J.; Facchetti, A.; Chang, R. P. H. *J. Phys. Chem. C* **2014**, *118*, 16967−16975.

(7) Yook, K. S.; Lee, J. Y. *Adv. Mater.* **2014**, *26*, 4218−4233.

(8) Chen, D.; Su, S.-J.; Cao, Y. *J. Mater. Chem.* **2014**, *2*, 9565−9578.

(9) Zhang, T.; Chu, B.; Li, W.; Su, Z.; Peng, Q. M.; Zhao, B.; Luo, Y.; Jin, F.; Yan, X.; Gao, Y.; Wu, H.; Zhang, F.; Fan, D.; Wang, J. *ACS Appl. Mater. Interfaces* **2014**, *6*, 11907−11914.

(10) He, X.; Cai, D.; Kang, D.-Y.; Haske, W.; Zhang, Y.; Zuniga, C. A.; Wunsch, B. H.; Barlow, S.; Leisen, J.; Bucknall, D.; Kippelen, B.; Marder, S. R. *J. Mater. Chem. C* **2014**, *2*, 6743−6751.

(11) Gaj, M. P.; Fuentes-Hernandez, C.; Zhang, Y.; Marder, S. R.; Kippelen, B. *Org. Electron.* **2015**, *16*, 109−112.

(12) Suzuki, Y.; Zhang, Q.; Adachi, C. *J. Mater. Chem. C* **2015**, *3*, 1700−1706.

(13) Mayr, C.; Lee, S. Y.; Schmidt, T. D.; Yasuda, T.; Adachi, C.; Brütting, W. *Adv. Funct. Mater.* **2014**, *24*, 5232−5239.

(14) Gong, Y.; Liu, J.; Zhang, Y.; He, G.; Lu, Y.; Fan, W. B.; Yuan, W. Z.; Sun, J. Z.; Zhang, Y. *J. Mater. Chem.* **2014**, *2*, 7552−7560.

(15) Huang, J.; Sun, N.; Yang, J.; Tang, R.; Li, Q.; Ma, D.; Li, Z. *Adv. Funct. Mater.* **2014**, *24*, 7645−7654.

(16) Chen, L.; Jiang, Y.; Nie, H.; Hu, R.; Kwok, H. S.; Huang, F.; Qin, A.; Zhao, Z.; Tang, B. Z. *ACS Appl. Mater. Interfaces* **2014**, *6*, 17215−17225.

(17) Choi, E. Y.; Mazur, L.; Mager, L.; Gwon, M.; Pitrat, D.; Mulatier, J. C.; Monnereau, C.; Fort, A.; Attias, A. J.; Dorkenoo, K.; Kwon, J. E.; Xiao, Y.; Matczyszyn, K.; Samoc, M.; Kim, D.-W.; Nakao, A.; Heinrich, B.; Hashizume, D.; Uchiyama, M.; Park, S. Y.; Mathevet, F.; Aoyama, T.; Andraud, C.; Wu, J. W.; Barsella, A.; Ribierre, J. C. *Phys. Chem. Chem. Phys.* **2014**, *16*, 16941−16956.

(18) Yook, K. S.; Lee, J. Y. *Adv. Mater.* **2012**, *24*, 3169−3190.

(19) Baumeier, B.; May, F.; Lennartz, C.; Andrienko, D. *J. Mater. Chem.* **2012**, *22*, 10971−10976.

(20) Kordt, P.; van der Holst, J. J. M.; Al Helwi, M.; Kowalsky, W.; May, F.; Badinski, A.; Lennartz, C.; Andrienko, D. *Adv. Funct. Mater.* **2015**, *25*, 1955−1971.

(21) Perucco, B.; Reinke, N.; Rezzonico, D.; Knapp, E.; Harkema, S.; Ruhstaller, B. *Org. Electron.* **2012**, *13*, 1827−1835.

(22) Mesta, M.; Carvelli, M.; de Vries, R. J.; van Eersel, H.; van der Holst, J. J. M.; Schober, M.; Furno, M.; Lüssem, B.; Leo, K.; Loebl, P.; Coehoorn, R.; Bobbert, P. A. *Nat. Mater.* **2013**, *12*, 652−658.

(23) van Eersel, H.; Bobbert, P. A.; Janssen, R. A. J.; Coehoorn, R. *Appl. Phys. Lett.* **2014**, *105*, 143303.

(24) Neumann, T.; Danilov, D.; Lennartz, C.; Wenzel, W. *J. Comput. Chem.* **2013**, *34*, 2716−2725.

(25) Ratcliff, L. E.; Grisanti, L.; Genovese, L.; Deutsch, T.; Neumann, T.; Danilov, D.; Wenzel, W.; Beljonne, D.; Cornil, J. *J. Chem. Theory Comput.* **2015**, *11*, 2077−2086.

(26) Mackerell, A. D. *J. Comput. Chem.* **2004**, *25*, 1584−1604.

(27) Kwiatkowski, J. J.; Nelson, J.; Li, H.; Bredas, J. L.; Wenzel, W.; Lennartz, C. *Phys. Chem. Chem. Phys.* **2008**, *10*, 1852−1858.

(28) Lukyanov, A.; Lennartz, C.; Andrienko, D. *Phys. Status Solidi A* **2009**, *206*, 2737−2742.

(29) May, F.; Al-Helwi, M.; Baumeier, B.; Kowalsky, W.; Fuchs, E.; Lennartz, C.; Andrienko, D. *J. Am. Chem. Soc.* **2012**, *134*, 13818−13822.

(30) Friederich, P.; Symalla, F.; Meded, V.; Neumann, T.; Wenzel, W. *J. Chem. Theory Comput.* **2014**, *10*, 3720−3725.

(31) Tao, Y.; Yuan, K.; Chen, T.; Xu, P.; Li, H.; Chen, R.; Zheng, C.; Zhang, L.; Huang, W. *Adv. Mater.* **2014**, *26*, 7930−79.

(32) Adachi, C. *Jpn. J. Appl. Phys.* **2014**, *53*, 060101.

(33) Jankus, V.; Data, P.; Graves, D.; McGuinness, C.; Santos, J.; Bryce, M. R.; Dias, F. B.; Monkman, A. P. *Adv. Funct. Mater.* **2014**, *24*, 6178−6186.

(34) Moral, M.; Muccioli, L.; Son, W.-J.; Olivier, Y.; Sancho-García, J. C. *J. Chem. Theory Comput.* **2015**, *11*, 168−177.

(35) Yu, M.; Wang, S.; Shao, S.; Ding, J.; Wang, L.; Jing, X.; Wang, F. *J. Mater. Chem. C* **2015**, *3*, 861−869.

(36) Yuan, W. Z.; Gong, Y.; Chen, S.; Shen, X. Y.; Lam, J. W. Y.; Lu, P.; Lu, Y.; Wang, Z.; Hu, R.; Xie, N.; Kwok, H. S.; Zhang, Y.; Sun, J. Z.; Tang, B. Z. *Chem. Mater.* **2012**, *24*, 1518−1528.

(37) ChemSpider. http://www.chemspider.com (accessed April 20, 2015), for the generation of chemical drawings.

(38) Sasabe, H.; Kido, J. *Chem. Mater.* **2011**, *23*, 621−630.

(39) Muccioli, L.; DAvino, G.; Berardi, R.; Orlandi, S.; Pizzirusso, A.; Ricci, M.; Roscioni, O. M.; Zannoni, C. In *Multiscale Modelling of Organic and Hybrid Photovoltaics*; Beljonne, D., Cornil, J., Eds.; *Top. Curr. Chem.*; Springer: Berlin Heidelberg, 2004; Vol. 352; pp 39101.

(40) In this work, we also enforced the united atom approximation to the hydrogen attached to carbazole (CBZ) nitrogen (NH atom-type in Table 1). This choice prevents the formation of a hydrogen bond; we thus discourage the adoption of our force field for carbazole in the presence of hydrogen bond acceptors.

(41) Tiberio, G.; Muccioli, L.; Berardi, R.; Zannoni, C. *ChemPhysChem* **2009**, *10*, 125−136.

(42) Vanommeslaeghe, K.; Hatcher, E.; Acharya, C.; Kundu, S.; Zhong, S.; Shim, J.; Darian, E.; Guvench, O.; Lopes, P.; Vorobyov, I.; Mackerell, A. D. *J. Comput. Chem.* **2010**, *31*, 671−690.

(43) Cornell, W. D.; Cieplak, P.; Bayly, C. I.; Gould, I. R.; Merz, K. M., Jr.; Ferguson, D. M.; Spellmeyer, D. C.; Fox, T.; Caldwell, J. W.; Kollman, P. A. *J. Am. Chem. Soc.* **1995**, *117*, 5179.

(44) Pizzirusso, A.; di Pietro, M. E.; de Luca, G.; Celebre, G.; Longeri, M.; Muccioli, L.; Zannoni, C. *ChemPhysChem* **2014**, *15*, 1356−1367.

(45) Reva, I.; Lapinski, L.; Chattopadhyay, N.; Fausto, R. *Phys. Chem. Chem. Phys.* **2003**, *5*, 3844−3850.

(46) Hénin, J.; Chipot, C. *J. Chem. Phys.* **2004**, *121*, 2904−2914.

(47) Weiner, S. J.; Kollmann, P. A.; Case, D. A.; Singh, U. C.; Ghio, C.; Alagona, G.; Profeta, S.; Weiner, P. *J. Am. Chem. Soc.* **1984**, *106*, 765−784.

(48) Yang, L. J.; Tan, C. H.; Hsieh, M. J.; Wang, J. M.; Duan, Y.; Cieplak, P.; Caldwell, J.; Kollman, P. A.; Luo, R. *J. Phys. Chem. B* **2006**, *110*, 13166−13176.

(49) von Lilienfeld, O. A.; Andrienko, D. *J. Chem. Phys.* **2006**, *124*, 054307.

(50) Wang, J.; Wolf, R. M.; Caldwell, J. W.; Kollman, P. A.; Case, D. A. *J. Comput. Chem.* **2004**, *25*, 1157.

(51) Perdew, J. P.; Ernzerhof, M.; Burke, K. *J. Chem. Phys.* **1996**, *105*, 9982.

(52) Perdew, J. P.; Burke, K.; Ernzerhof, M. *Phys. Rev. Lett.* **1996**, *77*, 3865−3868.

(53) Zhang, Y.; Yang, W. *Phys. Rev. Lett.* **1998**, *80*, 890.

(54) Adamo, C.; Barone, V. *J. Chem. Phys.* **1999**, *110*, 6158−6170.

(55) Weigend, F.; Ahlrichs, R. *Phys. Chem. Chem. Phys.* **2005**, *7*, 3297−3305.

(56) Grimme, S.; Ehrlich, S.; Goerigk, L. *J. Comput. Chem.* **2011**, *32*, 1456−1465.

(57) Besler, B. H.; Merz, K. M., Jr; Kollman, P. A. *J. Comput. Chem.* **1990**, *11*, 431−439.

(58) Frisch, M. J.; Trucks, G. W.; Schlegel, H. B.; Scuseria, G. E.; Robb, M. A.; Cheeseman, J. R.; Scalmani, G.; Barone, V.; Mennucci, B.; Petersson, G. A.; Nakatsuji, H.; Caricato, M.; Li, X.; Hratchian, H. P.; Izmaylov, A. F.; Bloino, J.; Zheng, G.; Sonnenberg, J. L.; Hada, M.; Ehara, M.; Toyota, K.; Fukuda, R.; Hasegawa, J.; Ishida, M.; Nakajima, T.; Honda, Y.; Kitao, O.; Nakai, H.; Vreven, T.; Montgomery, J. A., Jr.; Peralta, J. E.; Ogliaro, F.; Bearpark, F.; Heyd, M.; Brothers, J. J.; Kudin, E.; Staroverov, K. N.; Kobayashi, V. N.; Normand, R.; Raghavachari, J.; Rendell, K.; Burant, A.; Iyengar, J. C.; Tomasi, S. S.; Cossi, J.; Rega, M.; Millam, N.; Klene, J. M.; Knox, M.; Cross, J. E.; Bakken, J. B.; Adamo, V.; Jaramillo, C.; Gomperts, J.; Stratmann, R.; Yazyev, R. E.; Austin, O.;

Cammi, A. J.; Pomelli, R.; Ochterski, C.; Martin, J. W.; Morokuma, R. L.; Zakrzewski, K.; Voth, V. G.; Salvador, G. A.; Dannenberg, P.; Dapprich, J. J.; Daniels, S.; Farkas, A. D.; Foresman, J. B.; Ortiz, J. V.; Cioslowski, J.; Fox, D. J. *Gaussian09*, revision A.01; Gaussian Inc.: Wallingford, CT, 2009.

(59) Neese, F. *Wiley Interdiscip. Rev.: Comput. Mol. Sci.* **2012**, *2*, 73−78.

(60) Phillips, J. C.; Braun, R.; Wang, W.; Gumbart, J.; Tajkhorshid, E.; Villa, E.; Chipot, C.; Skeel, R. D.; Kale, L.; Schulten, K. *J. Comput. Chem.* **2005**, *26*, 1781−1802.

(61) The atom types CW and N5 were introduced to identify proper and improper dihedrals of PTBI. Aside from this, they coincide with CY and N4 atom types.

(62) Charbonneau, G. P.; Delugeard, Y. *Acta Crystallogr., Sect. B* **1977**, *33*, 1586−1588.

(63) Gerkin, R. E.; Reppart, W. J. *Acta Crystallogr., Sect. C* **1986**, *42*, 480−482.

(64) Belsky, V. K.; Zavodnik, V. E.; Vozzhennikov, V. M. *Acta Crystallogr., Sect. C* **1984**, *40*, 1210−1211.

(65) Sun, Y.-H.; Zhu, X.-H.; Chen, Z.; Zhang, Y.; Cao, Y. *J. Org. Chem.* **2006**, *71*, 6281−6284.

(66) Low, P. J.; Paterson, M. A. J.; Yufit, D. S.; Howard, J. A. K.; Cherryman, J. C.; Tackley, D. R.; Brook, R.; Brown, B. *J. Mater. Chem.* **2005**, *15*, 2304−2315.

(67) Woźniak, K.; Kariuki, B.; Jones, W. *Acta Crystallogr., Sect. C* **1991**, *47*, 1113−1114.

(68) Avendano, C.; Espada, M.; Ocana, B.; Garcia-Granda, S.; Diaz, M.; Tejerina, B.; Gomez-Beltran, F.; Martinez, A.; Elguero, J. *J. Chem. Soc., Perkin Trans. 2* **1993**, 1547−1555.

(69) Sobolev, A. N.; Belsky, V. K.; Romm, I. P.; Chernikova, N. Y.; Guryanova, E. N. *Acta Crystallogr., Sect. C* **1985**, *41*, 967−971.

(70) In the case of a relatively small isotropic box deformation, $l_s^i = \lambda l_e^i$ or $l_s^i = (1 + x)l_e^i$ with $x = \lambda - 1$ and $|x| \ll 1$, F becomes approximately equal to $|x|$. In fact, for this particular case, $V_s = (1 + x)^3 V_e$, $\Delta_{vol} = (1/3)|V_e - V_e(1 + x)^3|/V_e = (1/3)|3x + 3x^2 + x^3|$, and $\Delta_{def} = (1/3)(3|x| + 3|x|^2 + 3|x|^3)$. For small $|x|$, thus, we have Δ_{vol} and $\Delta_{def} \simeq |x|$ and of course $F = (1/2)(\Delta_{vol} + \Delta_{def}) \simeq |x|$.

(71) D'Avino, G.; Muccioli, L.; Zannoni, C.; Beljonne, D.; Soos, Z. G. *J. Chem. Theory Comput.* **2014**, *10*, 4959−4971.

(72) Jurečka, P.; Černý, J.; Hobza, P.; Salahub, D. R. *J. Comput. Chem.* **2007**, *28*, 555−569.

(73) Grimme, S. *Wiley Interdiscip. Rev.: Comput. Mol. Sci.* **2011**, *1*, 211−228.

(74) Sherrill, C. D. *Acc. Chem. Res.* **2013**, *46*, 1020−1028.

(75) Sherrill, C. D.; Sumpter, B. G.; Sinnokrot, M. O.; Marshall, M. S.; Hohenstein, E. G.; Walker, R. C.; Gould, I. R. *J. Comput. Chem.* **2009**, *30*, 2187−2193.

(76) Olivier, Y.; Muccioli, L.; Zannoni, C. *ChemPhysChem* **2014**, *15*, 1345−1355.

(77) Pettersson, I.; Liljefors, T. *J. Comput. Chem.* **1987**, *8*, 1139−1145.

(78) Jorgensen, W. L.; Tirado-Rives, J. *J. Am. Chem. Soc.* **1988**, *110*, 1657−1666.

(79) Olivier, Y.; Muccioli, L.; Lemaur, V.; Geerts, Y. H.; Zannoni, C.; Cornil, J. *J. Phys. Chem. B* **2009**, *113*, 14102−14111.

(80) D'Avino, G.; Mothy, S.; Muccioli, L.; Zannoni, C.; Wang, L.; Cornil, J.; Beljonne, D.; Castet, F. *J. Phys. Chem. C* **2013**, *117*, 12981−12990.

(81) Agrawal, P. M.; Rice, B. M.; Thompson, D. L. *J. Chem. Phys.* **2003**, *118*, 9680−9688.

(82) Zhang, Y.; Maginn, E. J. *J. Chem. Phys.* **2012**, *136*, 144116.

(83) Marcon, V.; Raos, G. *J. Am. Chem. Soc.* **2006**, *128*, 1408−1409.

(84) Massaro, F. R.; Moret, M.; Bruno, M.; Aquilano, D. *Cryst. Growth Des.* **2013**, *13*, 1334−1341.

(85) Rohl, A.; Gay, D. *J. Cryst. Growth* **1996**, *166*, 84−90.

(86) Sigma Aldrich online catalogue. http://www.sigmaaldrich.com/catalog/ (accessed April 20, 2015), obtained experimental melting points.

(87) Vydrov, O. A.; van Voorhis, T. *J. Chem. Phys.* **2010**, *133*, 244103.

(88) Sure, R.; Grimme, S. *J. Comput. Chem.* **2013**, *34*, 1672−1685.

(89) Sinnokrot, M. O.; Sherrill, C. D. *J. Phys. Chem. A* **2004**, *108*, 10200−10207.

(90) Yang, J.; Hu, W.; Usvyat, D.; Matthews, D.; Schütz, M.; Chan, G. K.-L. *Science* **2014**, *345*, 640−643.

(91) Worle, M.; Losio, P. A.; Gunter, P. CCDC 298742 REHJAQ01, 2006; private communication.

(92) Song, W.-F.; Wu, Y.; Fan, Y.; Wang, Y.; Liu, Y. *Acta Crystallogr., Sect. E* **2009**, *65*, o2461.

(93) Peter, C.; Kremer, K. *Faraday Discuss.* **2010**, *144*, 9−24.

(94) Carbone, P.; Varzaneh, H. A. K.; Chen, X.; Müller-Plathe, F. *J. Chem. Phys.* **2008**, *128*, 064904.

(95) Hofmann, D. W. M.; Kuleshova, L. N. *Cryst. Growth Des.* **2014**, *14*, 3929−3934.